POLITECNICO DI MILANO

School of Industrial and Information Engineering

Automation and Control Engineering

IMPLEMENT OF A MEASURING SYSTEM FOR A VEHICLE AND ITS USE FOR IDENTIFYING VEHICLE AND TYRE UNKNOWN PARAMETERS

Advisor

PRO. EDOARDO SABBIONI

ING. MICHELE VIGNATI

ZHOU KAIHUI

796465

Academic Year 2014/2015

Abstract

Most of control systems are model-based. Parameters of the model (varying with time) must be estimated and unmeasured states must be estimated. Estimators and state observers must be implemented on purpose. Instrumented vehicles allow the study and development of these features. In this thesis, the development of a measuring system for a passenger car is presented, includes the measurements of CAN BUS (sensors available on-board) and additional sensors placed on the vehicle with the aim of developing and verifying estimations and state observers.

In particular, in the present thesis, estimations for tyre model parameters and state observers for sideslip angle estimation are proposed.

Keywords

Tyres; Data Acquisition; CAN BUS; Extended Kalman filter; State and parameter estimation; Modelling and simulation technology

Introduction

Numerical observers describing the handling behaviour of passenger cars are extensively used in the simulation and design of modern vehicles, in order to improve performances. Numerical analysis of vehicle lateral dynamics needs a valid experimental sessions: road test should be performed and the data be collected used to identify and validate a suitable vehicle model for estimating the response to different steering-wheel inputs. In this thesis, an on-car Data Acquisition System has developed to acquire data from the vehicle.

External sensors cannot be applied to production vehicles. The Data Acquisition system is specially built in laboratory to monitor the states of vehicle through many additional sensors. Sensors used in the developed system include: pressure transducers, accelerometers, speed sensor, IMU, and road Dynamometric hub. The system also picks the information from CAN BUS.

The existing data acquisition system, which include many sensors, has been completed by adding the acquisition of CAN BUS. A new CAN BUS connection has been developed to extend its capability that can get information from the vehicle communication bus.

Then, several tests have been performed to acknowledge the steady-state and transient performance of the vehicle, in particular two manoeuvres have been engaged. With the data logged by this on-board vehicle, unknown parameters like tyre parameters and sideslip angle are estimated by numerical observers.

In chapter 1 and chapter 2, the Data Acquisition System (DAQ) is introduced. A complete set up of measurement has been developed for a passenger car. The DAQ system is presented, it consists of sensors, DAQ measurement hardware and a computer with programmable software.

In chapter 3, some vehicle specific statements have been measured. For example, the location of centre of gravity, mass distribution, the steering ratio and the roll angle gradient.

In chapter 4 and chapter 5, unknown parameters estimation is presented, such as tyre parameters and sideslip angle. Based on the data from the DAQ system, the comparison between the numerical and experimental results are presented.

Contents

List of Figures

List of Tables

Chapter 1

State of the art

In recent years, modern vehicles have been equipped with ever more sophisticated electronics and control systems, such as the Anti-lock Braking System (ABS) and the Electronic Stability Program (ESP). With the implementation of these intelligent systems, vehicles have become safer to drive ([1]) with less involvement in fatal accidents ([2]). To develop this control systems, numerical observers are needed in order to estimate vehicle states that cannot be measured directly, e.g. sideslip angle, vehicle speed, and so on.

The improvement of the observers requires accurate and 'up-to-date' vehicle dynamic information not only from in-vehicle sensors, in Fig 1.1, but also some additional data from external sensors since the state estimated must be compared with real values in order to prove the effectiveness of the model on which they are based.

A Data Acquisition system can measure many useful data while the vehicle is moving. This experimental system, in the instrumented vehicle, allows to study further the operational behaviour of the vehicle and help engineers to develop and test effectiveness of the observers. Also, some unknown parameters like sideslip angle can be estimated to give a better management of vehicle dynamics.

1.1 The Data Acquisition System

To fulfil the requirements of an experimental vehicle, a Data Acquisition System (DAQ) has been developed and integrated into the laboratory vehicle. The first au-

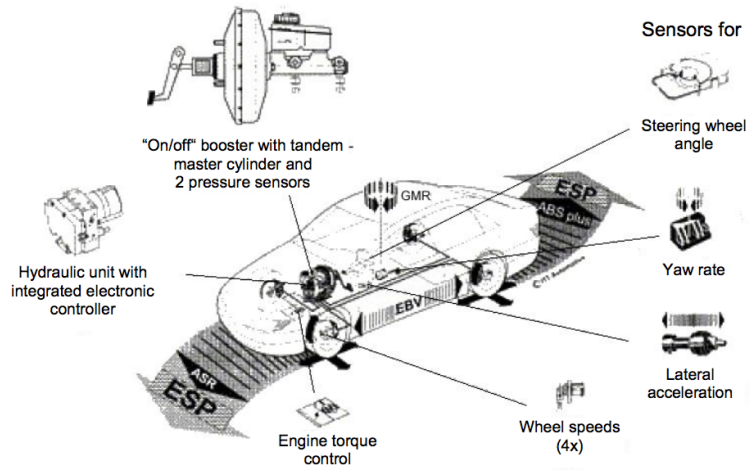

Figure 1.1: Sensor equipment of the vehicle

tomotive data acquisition system was used in crash tests in the 1970s. In 1976, the first data acquisition system travelled on-board the car during the test appeared in German. In 1996, the system fulfilled the requirements for hundreds of channels per test, it was also give a significantly reduce the size and mass of the on-board systems. Over the years data acquisition systems have been improved quite dramatically in performance and size.

Nowadays, Data acquisition system (Figure 1.2) has been wildly used in racing vehicles. Virtually every race car in competitions is equipped with computerized systems that help engineers, technicians and drivers to measure vehicle-physical parameters, understand and evaluate driver behaviour and his interaction with the car , and implement strategies to optimize overall performance. Usually measured quantities are: engine rotational speed (RPM), lateral and longitudinal acceleration, vehicle speed, track position, and steering angle. These quantities are examined in the context of race car. Also, DAQ is the key part of any race teams or vehicle manufacturers. It is vital to the development phase of a vehicle, so that designs can be validated and tunable parameters adjusted to increase performance and efficiency. In normal passenger cars, there are lots of data that can provide useful information to engineers and drivers in order to improve the vehicle performance, such as: sideslip angle, lateral speed and yaw rate.

The integration with Controller Area Network (CAN) BUS provides an inexpen-

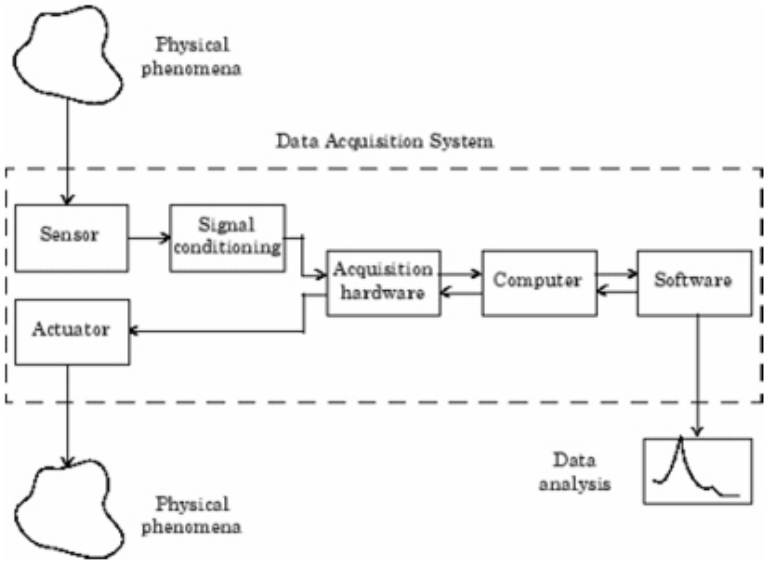

Figure 1.2: Data Acquisition System usage

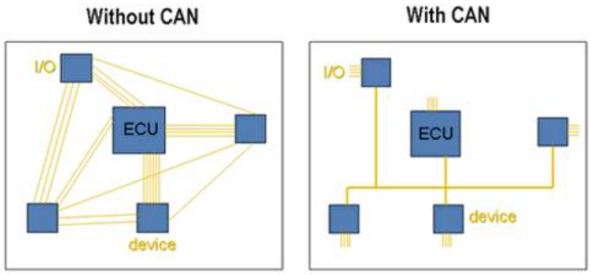

Figure 1.3: CAN networks simplify wiring between the many devices connected on the network.

sive, durable network that helps multiple CAN devices communicate with each other (Figure 1.3). This decreases overall cost and weight in automotive.

Logging on-vehicle data can include many different types of measurements and information, but one of the main pieces of in-vehicle data is traffic from CAN BUS. Messages conveying information about the current state of the vehicle (i.e. vehicle speed, engine speed, steer angle) are transmitted and read by electronic devices connected to the CAN BUS. Interfacing to the bus to log and analyse the CAN data allows for a better understanding of how the vehicle is operating and for further examination of the data.

1.2 Unknown data estimation

The automotive industry has made significant technological progress over the last decade, for example, concerning active vehicle stability control. Effective operation of each of these systems depends on an accurate knowledge of the vehicle states, such as velocity, lateral acceleration, yaw rate, as well as vehicle and tyre side slip. The data from DAQ system can provide a trustful information to analyse the other unknown data.

In this thesis a procedure to determine Tyre Cornering stiffness is presented according to Pacejka's MF-Tyre model ([3]), which is one of the most commonly used tyre model for handling simulations. The single-track vehicle model is implemented and used in the estimation process. With outdoor tests like steering pad and steer sweep, a methodology that is least square method ([4],[5]) for identifying the MF coefficients for the cornering condition is presented, based on the measurements carried out on-board vehicle during the tests.

As is well known, the direct measurement of vehicle sideslip ([6],[7],[8]) angle requires a complex experimental set-up (an optical device might be used) which does not appear to be suitable for implementation on ordinary passenger cars. Thus, this quantity has to be estimated starting from the measurements of vehicle lateral and longitudinal acceleration, speed and steer angle.

Several strategies were proposed ([9],[10]), mainly based on state observers and Extended Kalman Filter (EKF). Extended Kalman filter uses a priori knowledge about the system and noise acting on the system and they have proven to be robust to parameter changes. After the tyre parameters are correctly identified, the EKF can lead to the estimation of sideslip angle.

Chapter 2

Data Acquisition system

Most of the control systems are model based, but the parameters of the models have to be obtained on-board based on available measurement. A Data Acquisition (DAQ) system has been developed in order to:

1. Acquire all the information needed to develop model based observers;
2. Estimate vehicle unknown parameters;
3. Verify performances of implemented observers.

2.1 The test vehicle

The test vehicle is FIAT CROMA 1.9 JTD (Figure 2.1). The FIAT CROMA is a segment D passenger car. The standard vehicle dynamics controller comes from Bosch is fully managed by an electronic control unit. And the ABS + ESP are also equipped in the vehicle. The braking system is the power assisted hydraulic type. All the systems and the vehicle dynamics controllers in vehicle are available for the tests. The Table 2.1 shows some basic configurations of FIAT CROMA.

Table 2.1: Basic values of FIAT CROMA

Model	1.9 MultiJet 16V	Class	Large family car
Body style	5-door estate	Transmission	6-speed manual
Engine	l4 DOHC 16V	Displacement	1910cc
Power	110kw	Torque	320N· m

Figure 2.1: FIAT CROMA

2.2 Scheme of the system

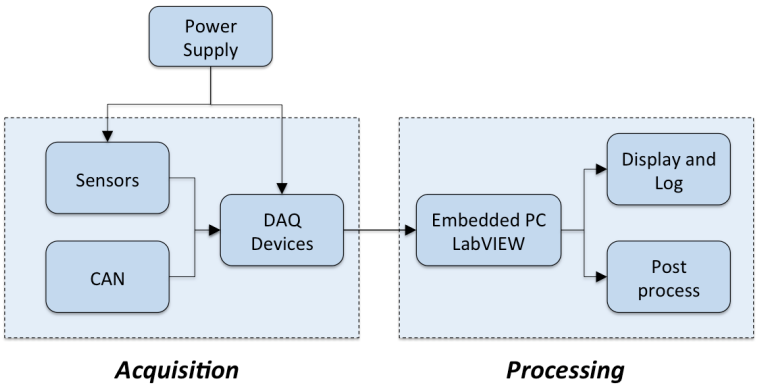

Figure 2.2: Data Acquisition system

Figure 2.2 shows the Data Acquisition system. It is used to monitor various parameters related to the vehicle dynamic performance:

1. Measure driver input signals: Steer angle; Brake pressure; Engine speed and torque;
2. Measure vehicle dynamics responses: Vehicle speed and angular rates; Wheel speed; Sideslip angle; Tyre-road contact forces

In the acquisition part, a power unit provides power to the sensors and DAQ devices. External sensors and CAN BUS on board can acquire data while car is running and transmit them to DAQ devices. DAQ device synthesizes all the signals, also operates the signal conditioning in real-time.

The data are transferred through vehicle network communications and then processed in LabVIEW by an embedded PC. All the data can be displayed in the front panel of the software, while the logged data can be stored into the file. In the post process, the data transforms into the engineering units for future analysis.

2.3 List of sensors

The test car is equipped with a full set measurements are shown in the Table 2.2.

Table 2.2: Sensors in the car

Measuring device	Measured variable
Accelerometers	Acceleration along longitudinal and vertical Acceleration along each wheel Acceleration along hub and upper mount
Pressure sensor	Brake pressure front left Brake pressure front right Brake pressure rear left Brake pressure rear right
Inertial Measurement	longitudinal, lateral and vertical acceleration Yaw, roll and pitch rate
Road Dynamometric hub	Forces and moments along x, y and z axle Wheel angle position Wheel rolling velocity
Correvit datron	Longitudinal velocity Lateral velocity Sideslip angle
CAN BUS	Steering wheel angle Engine speed and torque Gas position ABS, MSR, ASR, VDC signals

Figure 2.3: Accelerometers on front right hub

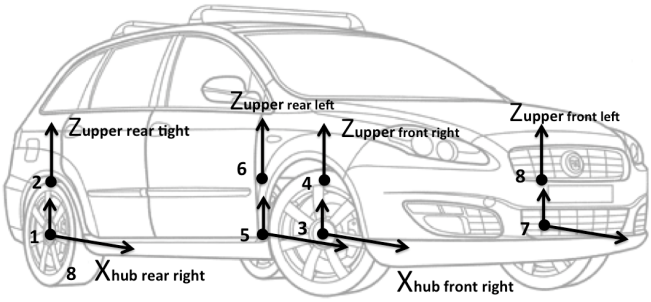

Figure 2.4: The placement of the accelerometers

2.3.1 Accelerometer

An accelerometer in Figure 2.3 measures proper acceleration. The purpose of the accelerometer is to measure vibration transmission for comfort estimation.

The Kistler K-shear piezo voltage (Type 8702) accelerometer has an internal microelectronic piezoelectric signal conditioning circuit converts the charge developed in the quartz element as a result of the accelerometer being subjected to a vibration, into a usable high level voltage signal at a low impedance output. The data sheet of the accelerometer is shown in Table 2.3.

The accelerometers are placed on the hubs and upper mounts of the test car, contains two modes that has installed in the vehicle, the one with range 25g (sensi-

tivity is 200 mV/g), is placed at hub in vertical z direction, the other one with range 50g (sensitivity is 100 mV/g), is placed at hub in longitudinal x direction and upper mount in vertical z direction. The placement of the accelerometers is labelled in Figure 2.4. The different numbers show the different accelerometers have been mounted on the car, with the respective directions of reference.

Table 2.3: The data sheet of the accelerometers

Specification	Type 8702/4B50	Type 8702/4B25
Acceleration range	± 50 g	± 25 g
Acceleration limit	± 100 gpk	± 50 gpk
Transverse acceleration limit	± 100 gpk	± 50 gpk
Sensitivity	100 mV/g	200 mV/g
Frequency response	0.5...10000 Hz	1...8000 Hz
Ouput Voltage full scale	± 5 V	± 5 V
Number of sensors	1, 3, 5, 7 in longitudinal and 2, 4, 6, 8 in vertical	1, 3, 5, 7 in vertical

2.3.2 Pressure sensor

Pressure sensors are used to measure the pressure in a braking system. The four pressure sensors are fitted on the outlet of the brake hydraulic unit.

The Bosch pressure sensor RDS2 with a measurement range of 0 bar to 210 bar are fitted in all four wheel brake lines. Evaluation electronics inside the sensor convert the signals from the bridge circuit into an analogue output voltage between 0 V and 10 V.

The sensitivities and the offset of the sensors are recorded in Table 2.4.

Table 2.4: The data sheet of the pressure sensors

Sensors position	Sensitivity	Offset
Front left	62.5 bar/V	-41.2 bar
Front right	62.5 bar/V	-40.2 bar
Rear left	62.5 bar/V	-41 bar
Rear right	62.5 bar/V	-39.8 bar

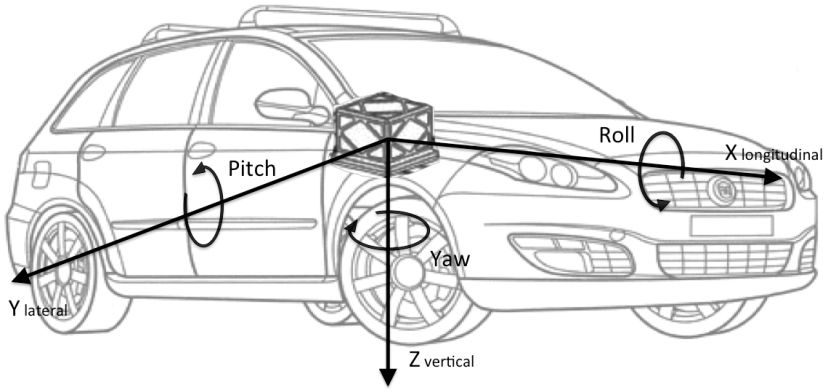

Figure 2.5: The placement of IMU

2.3.3 Inertial measurement unit

The gyroscopic sensor is to measure vehicle angular velocities (yaw, pitch and roll rate) and vehicle accelerations (A_x, A_y, A_z).

The IMU 3F-3C from INERTIAL DYNAMICS is a complete 6-degrees-of-freedom inertial measurement unit. It is calibrated for operation over its temperature range of -30 °C to +70 °C. It performs accurately with angular rates up to ±300 °/s and accelerations up to ±10 g. IMU 3F-3C uses three fibre optic angular rate giro (Sagnac effect) with high stability and low noise over time. Three open loop capacitive accelerometers give an accurate true static response up to 180 Hz.

In an ideal case, the gyroscopic sensor is attached precisely in the position of the center of gravity of the vehicle. The gyroscopic sensor is placed as close as possible to the center of gravity shown in Figure 2.5, where just behind the gear selector lever. Besides, the sensitivity of IMU is shown in Table 2.5.

Table 2.5: The output sensitivity of IMU

Acceler	Sensitivity	Gyro	Sensitivity
X	5.91236 $(m/s^2)/V$	Roll	17.99 (deg/s)/V
Y	5.94342 $(m/s^2)/V$	Pitch	17.39 (deg/s)/V
Z	5.82689 $(m/s^2)/V$	Yaw	18 (deg/s)/V

Figure 2.6: dynamometric hub

2.3.4 Wheel dynamometric hub

The dynamometric hub (Figure 2.6) is a wheel force sensor, for which measures three forces and moments on a rotating wheel. The hub is mounted on the left front wheel, measures multi-axial loads imposed on the vehicle by the pavement.

The dynamometric hub S630 of RoaDyn System 1000 from Kilster has four load cells. Each load cell supplies three measuring signals according to the load components F_x, F_y and F_z. Signal conditioning is carried out on miniature PC boards in the load cells. For each load cell, the three force signals together with identification and calibration data are fed via a cable with a 9-pole miniature connector to the connector carrier of the hub electronics. The sensitivities for the signals are shown in the following Table 2.6:

Table 2.6: The sensitivities of dynamometric hub

F_x	2000 N/V	M_x	400 Nm/V
F_y	2000 N/V	M_y	400 Nm/V
F_z	2000 N/V	M_z	400 Nm/V
Angle	50 deg/V	Wheel speed	19.47 (Km/h)/V

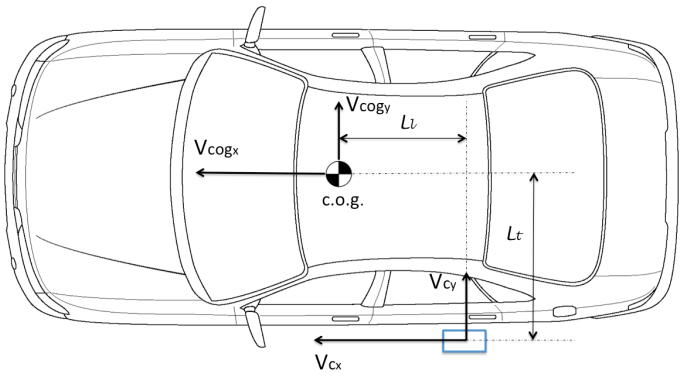

Figure 2.7: Velocity correction

2.3.5 Speed sensor

To determine the vehicle longitudinal, lateral velocity and sideslip angle, a speed sensor is used.

The speed sensor from Correvit Datron is a non-contact velocity measurement system which can determine both the longitudinal and also the lateral velocity of the vehicle. With the help of a lamp, a spot of light is projected onto the road surface. The reflected light manifests a statistical distribution of light and dark spots of the road surface structure. As a result of the movement of the vehicle across the surface, the light/dark contract spots are modulated in such a way that a velocity proportional frequency can be measured in the sensor.

As assembly of the Correvit sensor precisely at the center of gravity of the vehicle is not possible, it is attached to the vehicle door side as shown in Figure 2.7. Velocities have to be corrected in order to consider the distance from Datron to c.o.g. and yaw rate:

$$V_{cog_x} = V_{cx} - l_t \cdot \dot{\psi} \tag{2.1}$$

$$V_{cog_y} = V_{cx} - l_l \cdot \dot{\psi} \tag{2.2}$$

V_{cog_x} and V_{CoG_x} represent the longitudinal and lateral velocities locating at the c.o.g., V_{cx}, V_{cx} stand for the longitudinal and lateral velocities locating at the Datron. The distance along longitudinal axle between the center of gravity and Datron is l_l and distance along transverse axle between the center of gravity and Da-

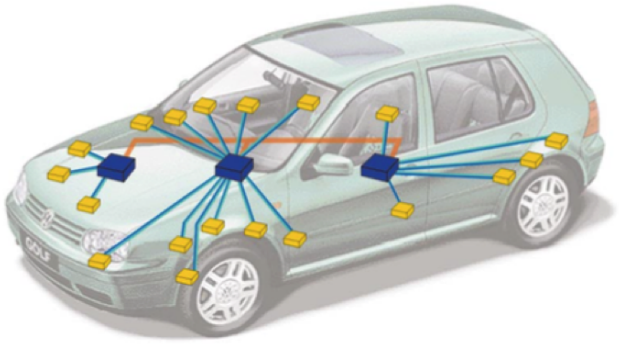

Figure 2.8: CAN BUS network

tron is l_t.

2.3.6 CAN BUS

The on-vehicle Data Acquisition system can log many different measurements and information from sensors, but also, messages conveying information about current state of vehicle (i.e. vehicle speed, engine speed and etc) in CAN BUS can be obtained simultaneously.

To achieve the CAN BUS signal, a twisted-pair cable was made to connect the CAN BUS panel unit where under the steering pad. With an 9-pin D-sub connector include CAN _Low and CAN_High, signals can successfully transmit from vehicle to Data Acquisition module. After CAN data sheet specific to FIAT CROMA been downloaded into the DAQ device, all the signals from CAN BUS can be readable in the engineering units.

CAN is a 2-wire, multi-drop serial bus over which devices connected to the network (Figure 2.8) communicate with each other. The use of a CAN BUS system in a car makes it possible to link different electronic modules together.

The data frame is the fundamental unit of data transfer on a CAN network. Figure 2.9 shows a simplified view of the CAN data frame. When multiple CAN devices transmit a frame at the same time, the identifier (ID) resolves the collision. The highest priority ID continues, and the lower priority IDs retry immediately afterwards. The ISO 11898 CAN standard specifies two ID formats: the standard format of 11 bits and the extended format of 29 bits. The ID is followed by a length code that specifies the number of data bytes in the frame. The length ranges from

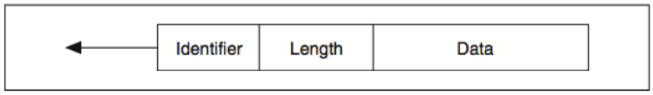

Figure 2.9: Can ID message

0 to 8 data bytes. The ID value determines the meaning of the data bytes.

The CAN BUS system is divided into 3 special systems due to the different requirements of repetition rate and the data volume:

1. Drive train CAN BUS (high-speed) at 500 kbps with real time requirements, include engine control unit, brake control unit and so on;
2. Infotainment CAN BUS (low-speed) at 100 kbps with low time, include radio unit and so on;
3. Convenience CAN BUS (low-speed) at 100 kbps with low time requirements, include climate control unit, door control unit and so on;

2.4 DAQ devices

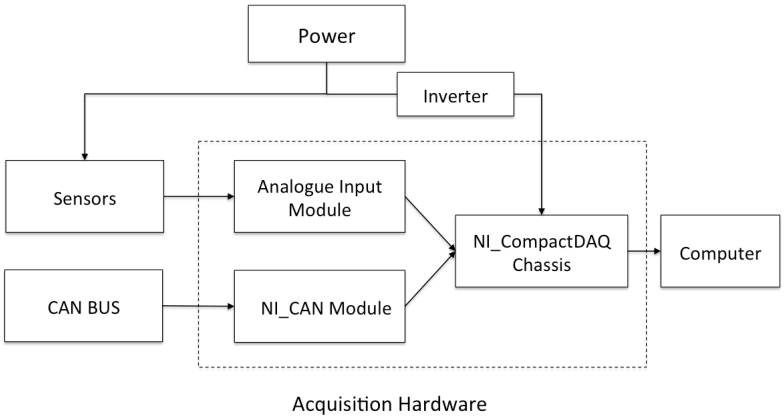

Figure 2.10: The Data Acquisition hardware scheme

Figure ?? shows the scheme of the DAQ hardware. After signals gained from sensors and CAN BUS, they transmit into NI-modules, which have already installed in the slots of the NI CompactDAQ chassis.

Figure 2.11: The Data Acquisition System on-board

A storage battery is mounted in the trunk, output a 12V DC power, providing suitable power to all external sensors. The battery is connected to the main battery in the vehicle, so it can be charged when vehicle is moving. Also, an inverter that convert DC to AC is placed in vehicle, it supplies the NI CompactDAQ device directly.

The analogue input modules are the terminal of sensors signals. Each module features built-in signal conditioning and direct signal connection with relative sensor. All A/D and D/A conversion happens in the module before the data reaches the chassis.

The NI_CAN module NI 9862 works for applications requiring high-speed manipulation of CAN frames and signals.

The NI CompactDAQ 9178 chassis is a portable, rugged data acquisition platform that integrates connectivity and signal conditioning into modular I/O. The whole system in the trunk is in Figure 2.11.

2.5 Computer program

There are many sensors in the car as the external measurement devices, about 50 channels (Table 2.7) in total including sensors signals and CAN BUS signals.

Table 2.7: LabVIEW channels

Channel	Signal	Channel	Signal
1	Time	26	DYNHUB_FL_AS
2	HUBRR_AZ	27	DYNHUB_FL_VS
3	HUB_RR_AZ	28	DATRON_VX
4	HUB_RL_AX	29	DATRON_VY
5	HUB_RL_AZ	30	DATRON_BETA
6	DOM_FR_AZ	31	STEER_ANGLE
7	DOM_FL_AZ	32	GPS
8	DOM_RR_AZ	33	CAN_AX
9	DOM_RL_AZ	34	CAN_AY
10	BRAKE_FR_PRUESSURE	35	CAN_YAW_RATE
11	BRAKE_FL_PRUESSURE	36	CAN_STEERING_WHEEL_ANGLE
12	BRAKE_RR_PRUESSURE	37	CAN_ENGINE_SPEED
13	BRAKE_RL_PRUESSURE	38	CAN_ENGINETORQUE
14	IMU_AZ	39	CAN_GASPEDALPOSITION
15	IMU_AY	40	CAN_ABS
16	IMU_AX	41	CAN_MSR
17	IMU_YAW	42	CAN_ASR
18	IMU_PITCH	43	CAN_VDC
19	IMU_ROLL	44	CAN_MASTERCYLINDERPRESSURE
20	DYNHUB_FL_FX	45	CAN_THROTTLE_POSITION
21	DYNHUB_FL_FY	46	CAN_LF_WHEEL_SPEED
22	DYNHUB_FL_FZ	47	CAN_RF_WHEEL_SPEED
23	DYNHUB_FL_MX	48	CAN_RF_WHEEL_SPEED
24	DYNHUB_FL_MY	49	CAN_RR_WHEEL_SPEED
25	DYNHUB_FL_MZ	50	CAN_VEHICLESPEED

The NI hardware DAQ and NI_CAN are applied under LabVIEW software. The software provides full-featured Application Programming Interfaces (APIs). The CAN and DAQ are programmed in the same CompactDAQ chassis at the same time.

The method is that use the NI-XNET ports in order to share a common time-base with other modules, so it can allow a better correlation of data and traffic from the chassis. Also, the user can route the Start Trigger between multiple DAQ and CAN modules. For example, using the appropriate property nodes, the Start Trigger of an analogue input DAQ module can be used as a CAN interface Start Trigger (Figure 2.12). So this can be used as the synchronize with the different data

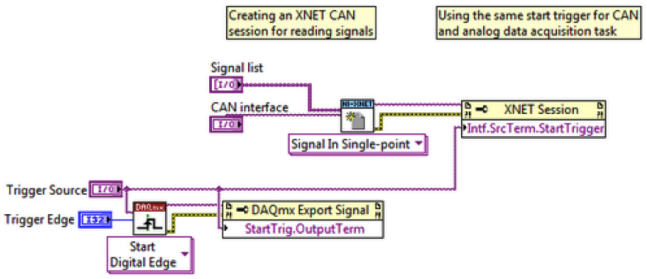

Figure 2.12: CompactDAQ and NI_CAN synchronization

flow in DAQ and CAN.

2.5.1 Data log and display

The front panel of LabVIEW is designed as a user interface by placing controls and indicators on it. After supply inputs, the user can see the results in the indicators. Controls define inputs and indicators display outputs. The window is an interface for users, there are several folders in Figure 2.13 showing different classified signal:

- The front panel is shown . The first screen shows the speed gauge, the longitudinal, lateral acceleration and the sideslip angle. Moreover, also the alarm light ABS, MSR, VDC, ASR will turn on when these systems are active;
- The second folder gives the IMU signals, which are three accelerations along three axles and its yaw, pitch and roll rate. Also, the longitudinal and lateral speed, sideslip angle are showed in this screen;
- The third folder is about the 3-axis forces and torques signals on the left front wheel from the dynamometric hub;
- In the forth folder, the accelerations signals in the hubs and upper mounts on the suspension structure are showed in the fourth page. In this page also contains the bake pressure in four wheels;
- The front CAN panel in fifth page is showing engine speed and torque, vehicle longitudinal speed and cornering wheel angle from CAN BUS;

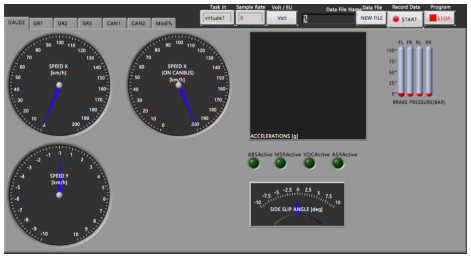

(a) First folder

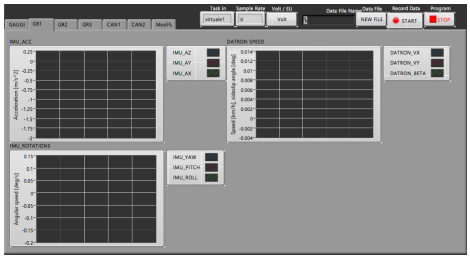

(b) Second folder

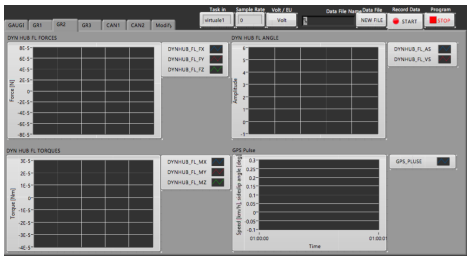

(c) Third folder

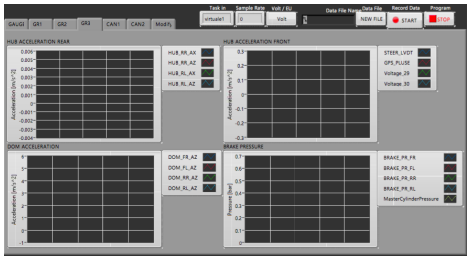

(d) Fourth folder

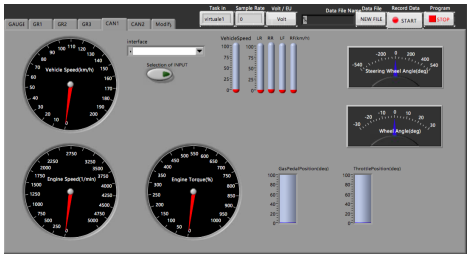

(e) Fifth folder

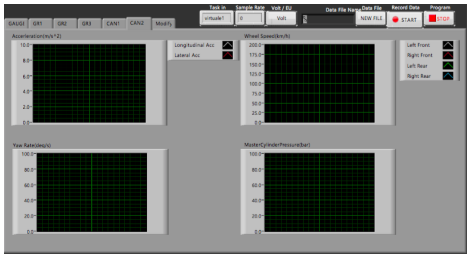

(f) Sixth folder

Figure 2.13: The front panel

- The sixth page shows the master cylinder pressure and longitudinal and lateral acceleration;
- The seventh page in Figure 2.14 is a modification panel that can apply a new sensibility and a new offset. Also, the other messages from CAN BUS can be re-chosen to read through this window.

There are mainly three steps on this program, which are acquiring, displaying and storing. The DAQ devices acquire data from different sensors at a given sampling rate defined by user. For example, if the dynamic performance is required, it can be set as 100 Hz. If the suspension acceleration for comfort test is required, it can be set as 2000 Hz. Meanwhile, due to the synchronize connection between DAQ and CAN BUS, the data can be acquired at the same time because of the Start

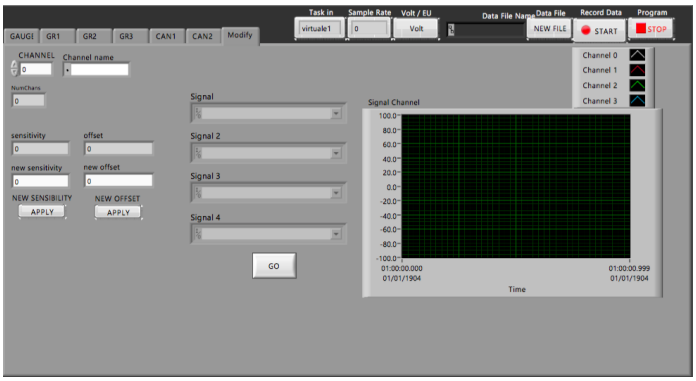

Figure 2.14: The seventh panel

Trigger.

Within one data flow, all the signals appear as analogous values with different columns enter from the input terminal port. The cycle producer who acquires the data from the card and puts them into cycle consumer, who contains two queues, one for writing to files (optional) and the other one for the screen reading. If the recording bottom is active, data are written to file, otherwise the queue is empty. Using the queue function block, the data can be stored while the program is running. The different displaying indicators in the front panel can give engineers a good interface interaction.

2.6 Postprocess

The results of the on board system are shown in MATLAB graphs. The channel been selected is displayed in y axis, the x axis displays the Time lapse. A process of filter function also plants into the program. It makes a good comparison between the raw data and the filtered data.

In a sweep manoeuvre in Figure 2.15. During this test, the longitudinal speed was kept around 50 km/h. From Figure 2.15a and Figure 2.15b show the yaw rate signal obtained from different sensors, one is recorded from IMU (include filtered at 4 Hz) and the other one is recorded from CAN BUS, but the differences between these two signals are very small, because the DAQ and CAN are running in the same timebase. Figure 2.15c shows the lateral velocity from Datron and Figure 2.15d shows the lateral force from Dynamometric hub.

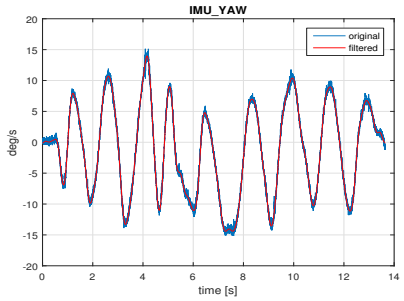

(a) Yaw rate from IMU (include filtered at 4Hz)

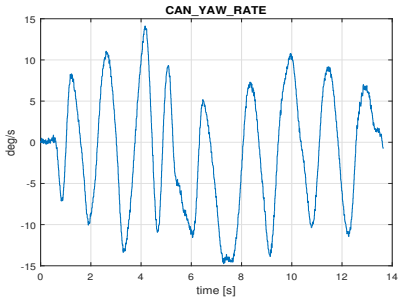

(b) Yaw rate from CAN BUS

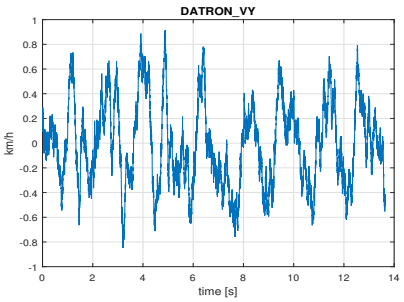

(c) Lateral velocity from Datron

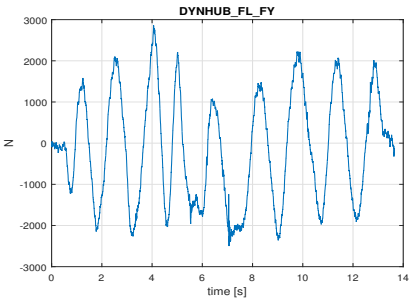

(d) Lateral force from Dynhub

Figure 2.15: Sweep singles in display

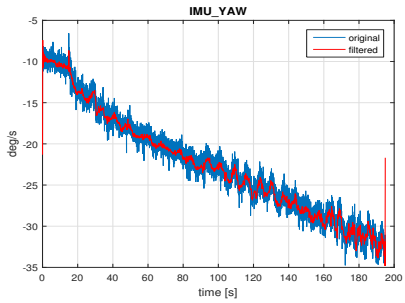

(a) Yaw rate from IMU (include filtered at 4Hz)

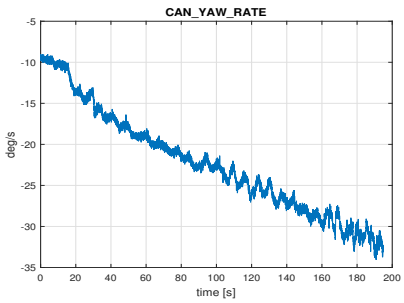

(b) Yaw rate from CAN BUS

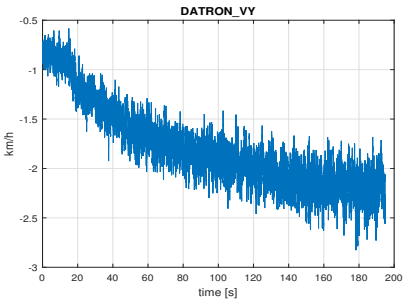

(c) Lateral velocity from Datron

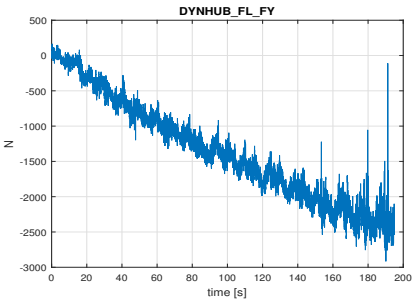

(d) Lateral force from Dynhub

Figure 2.16: Steady-pad singles in display

In a steady-state manoeuvre in Figure 2.16. The car performed a steady-state cornering, under slowly increasing the cornering speed, with a high value of lateral acceleration. It can be observed that the yaw rate signals from IMU and CAN BUS (Figure 2.16a and Figure 2.16b) are almost consistent with each other, reached the final value of 33 deg/s. The lateral velocity reached 2.2 km/h at the end in Figure 2.16c. And the lateral force reached 2450 N at the same time is shown in Figure 2.16d.

Chapter 3

Estimation of vehicle unknown parameters

In order to produce the complete vehicle simulation model, some vehicle-specific data must be known. For this reason, the location of center of gravity, the steering ratio and the roll angle gradient are determined experimentally. Below, the individual test and the implementation of the measurements are described.

3.1 Location of center of gravity

The location of center of gravity from the test vehicle is determined in longitudinal, lateral and vertical direction. In Figure 3.1, this is made according to a reference that x axis is the longitudinal axis of the vehicle, z axis is perpendicular to the ground in downward direction and the y axis is taken perpendicular to x and z considering in right hand principle property.

The coordinates of the center of gravity in the x and y directions are determined by measuring the four-wheel loads by means of 4 balances, over which the vehicle is placed. It assumes the vehicle is completely static while the forces are measured in a horizontal plane.The Table 3.1 shows the result:

Table 3.1: Vehicle vertical load

Front left load	506 kg	Front right load	458 kg
Rear left load	347 kg	Rear right load	380 kg

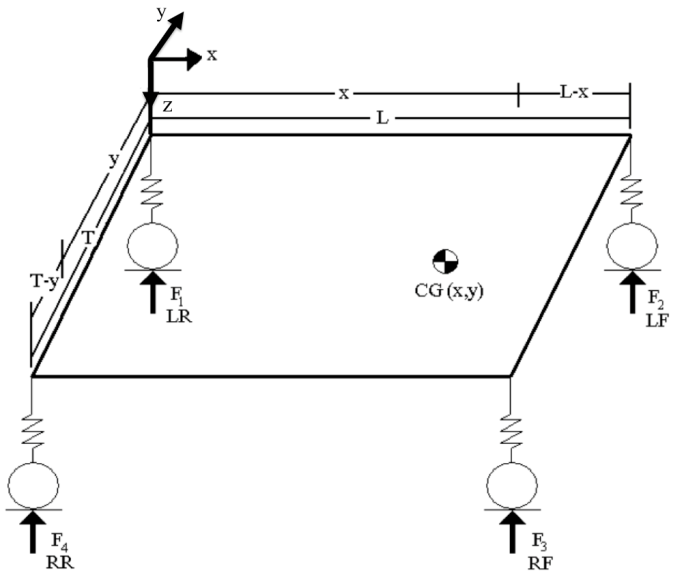

Figure 3.1: Force diagram of a vehicle

Alongside the overall weight of the vehicle is determined. The position of the center of gravity in x and y direction can be calculated with the known wheel base length and track width variables by moment equilibrium. Figure 3.1 shows the force diagram of a stationary vehicle. Considering the car as a rigid body, the equilibrium equations are:

$$\sum F_z = F_1 + F_2 + F_3 + F_4 = mg \tag{3.1}$$

$$\sum M_x = (F_1 + F_2)y - (F_3 + F_4)(T - y) = 0 \tag{3.2}$$

$$\sum M_y = (F_2 + F_3)(L - x) - (F_1 + F_4)x = 0 \tag{3.3}$$

F_1 , F_2 , F_3 , F_4 are the normal forces at each wheel of the vehicle, x and y relate to the center of gravity CG, L and T are the wheelbase and track length of vehicle. From the Equation 2.1 the total mass of the vehicle is obtained:

$$m = \frac{\sum F_z}{g} = 1681\text{kg} \tag{3.4}$$

From the second Equation 2.2 and the third Equation 2.3 the x position and the y

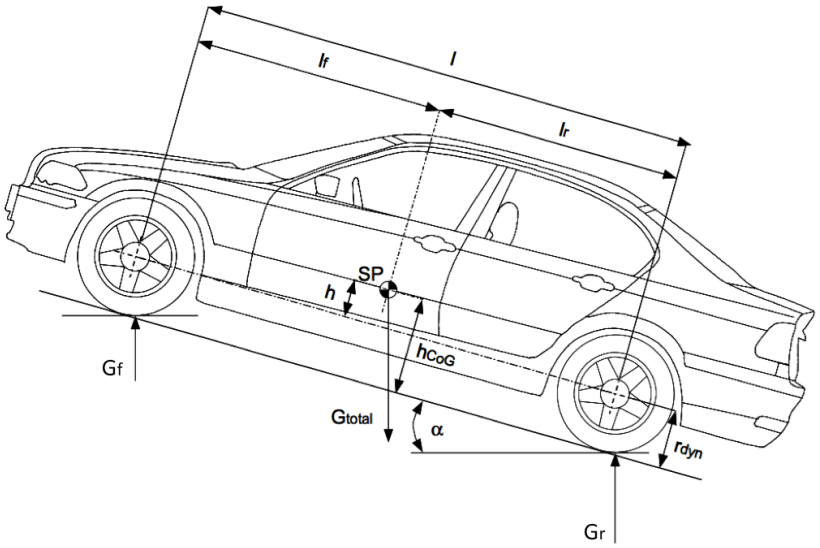

Figure 3.2: Measurement of the vehicle's center of gravity height h_{CoG}

position of the c.o.g. are obtained in following:

$$x = \frac{(F_2 + F_3)L}{F_1 + F_2 + F_3 + F_4} = 1540\text{mm} \tag{3.5}$$

$$y = \frac{(F_3 + F_4)T}{F_1 + F_2 + F_3 + F_4} = 750\text{mm} \tag{3.6}$$

The height of the center of gravity see Figure 3.2 is determined by weight displacement when lifting an axle. In this process, the parking brakes are engaged and the transmission is in neutral, through which the wheels can be freely turned.

To detect the rear axle load G_r, two balances are used to measure the rear axle load, placed at the left and right side individually. To measure the inclination angle α, an inclination sensor was fixed inside the car, always kept parallel with the vehicle longitudinal axle so as to get the right tilt angle same with the vehicle itself. From the experiments had preformed, obtained the rear axle load G_r=982 kg and inclination angle α=6.2° respectively, so it is possible to determine the z coordinate of the c.o.g.:

$$h_{CoG} = \frac{G_r l - G_{total} l_r}{tan(\alpha) \cdot G_{total}} + r_{dyn} = 580\text{mm} \tag{3.7}$$

The rolling wheel radius r_{dyn} is measured with the vehicle at a standstill. G_r and α

are the measured data, G_{total} is obtained by counting all vertical forces together, and l_f, l_r are got from data sheet of the vehicle.

Thus, the vehicle parameters obtained with described experimental procedures are reported in Table 3.2 and the graphic model of CROMA including the position of c.o.g. is in Figure 3.3.

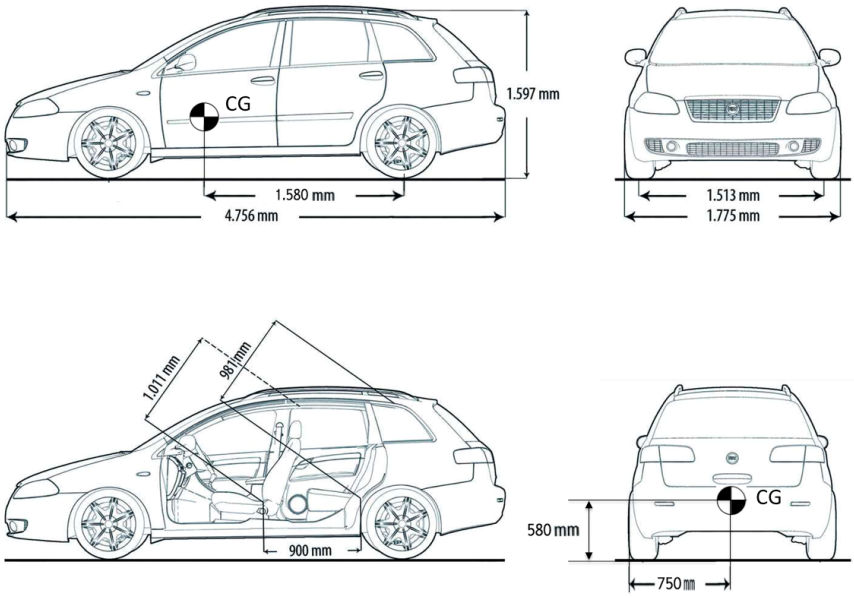

Figure 3.3: The demension of CROMA

Table 3.2: The dimension of CROMA

Wheel base	ρ	2700mm
Track width front	T_f	1514mm
Track width rear	T_r	1495mm
Loaded radius	r_{dyn}	315mm
Total mass	m	1681kg
Distance front axle-center of gravity	l_f	1160mm
Distance rear axle-center of gravity	l_r	1540mm
Center of gravity height	h_{CoG}	580mm

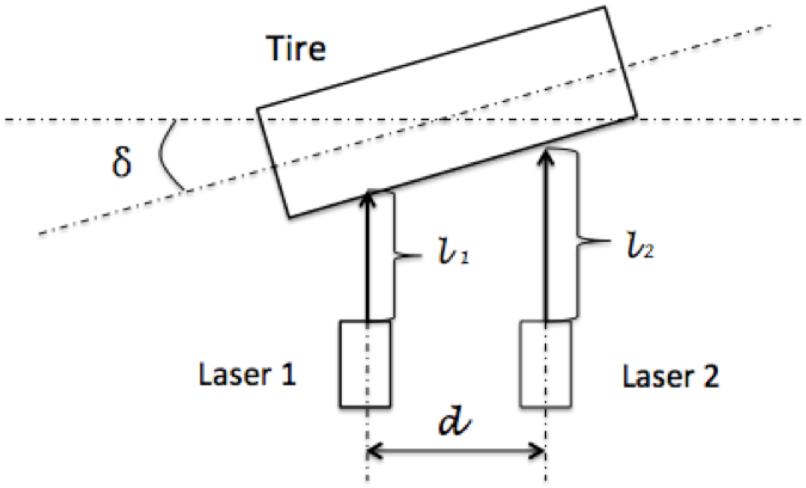

Figure 3.4: Steering ratio identification

3.2 Steering ratio definition

Steering ratio refers to the ratio between the turn of the steering wheel (in degrees) and the turn of the wheels (in degrees).

A Laser Distance Measuring Tool has been used. Pointing the laser distance measuring devices against a target, the device will give an output with correspond voltage. The configuration table of the laser device is in Table 3.3.

Table 3.3: M5L/200 Laser sensors

Type	Range (mm)	Reference Distance (mm)	Voltage (V)	Sensitivity (mm/V)
M5L/200	±100	340	±10	10

A method is implemented to calculate the steering ratio with the two laser devices. In the horizontal plane as the same height of wheel center, fixing two infra red rays against two points with certain distance d in Figure 3.4. Each side has one laser. Rotating the steering wheel with a number of fixed series degrees, while recording the different distance outputs l_1 and l_2 from two laser devices.

Table 3.4: Steering ratio measurement data

Tests	Steering wheel	Laser l_1	Laser l_2	Error	Wheel	Steering ratio
#	deg	mm	mm	mm	deg	-
1	-271.80	26.00	-64.00	0.90	14.23	-18.28
2	-229.40	17.50	-52.10	0.71	11.09	-19.54
3	-178.50	16.50	-39.90	0.58	9.03	-18.54
4	-140.80	14.50	-30.50	0.47	7.22	-17.89
5	-81.10	8.80	-18.30	0.28	4.37	-16.19
6	-40.30	-1.10	-8.00	0.07	1.11	-22.91
7	0.00	-7.85	-3.60	0.04	-0.69	0
8	44.90	-12.90	6.00	0.20	-3.05	-18.69
9	0.80	-23.40	12.00	0.37	-5.69	-17.98
10	132.20	-37.40	18.00	0.57	-8.87	-16.07
11	192.68	-51.60	27.30	0.80	-12.53	-16.21
12	230.00	-62.60	34.20	0.96	15.25	-15.75
13	274.80	-81.20	38.80	1.14	18.68	-15.24

So the relation formula is:

$$\delta = \arctan\left(\frac{l_2 - l_1}{d}\right) \tag{3.8}$$

where δ is the wheel turn angle. According to the data in Table 3.4, the steering wheel data are read from CAN BUS, and wheel rotation data are got from the triangular calculation. The errors are gained from the amplitude jitter from the output of the laser devices. In total, the steering ratio can get:

$$Steering\,ratio_{mean} = \frac{\delta_{Steering\,wheel\,deg}}{\delta_{wheel\,deg}} \tag{3.9}$$

Considering errors, the diagram shows in Figure 3.5. The diagram shows almost a linear relation between the steering wheel angle and wheel angle. The dot data can be fitted to a linear line trough MATLAB, the correlation coefficient can

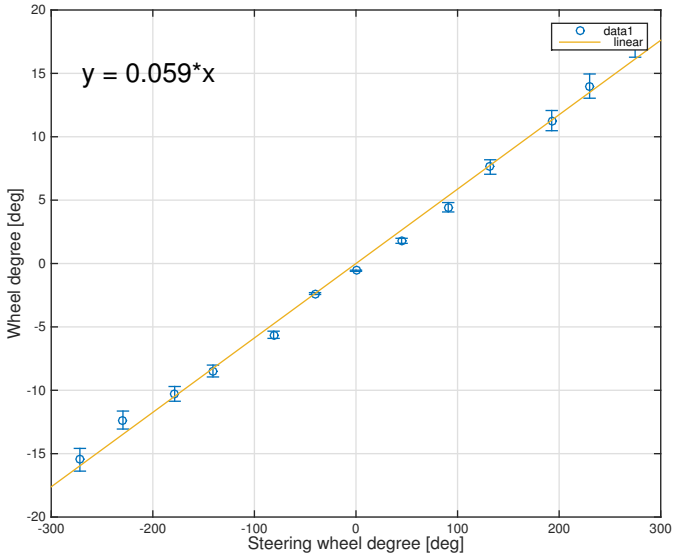

Figure 3.5: Error diagram

be calculated as:

$$R = \frac{\sum_{i=1}^{n}(x_i - \bar{x})(y_i - \bar{y})}{\sqrt{\sum_{i=1}^{n}(x_i - \bar{x})^2}\sqrt{\sum_{i=1}^{n}(y_i - \bar{y})^2}} = 0.9977 \tag{3.10}$$

From this data, it can be seen a good linear correlation (dependence) between two variables. So the linear part as shown:

$$y = 0.59 * x \tag{3.11}$$

The gradient of the fitting line is the inverse of the steering ratio. So the steering ratio is $1/0.59 = 17$.

3.3 Estimation of the Roll gradient

The lateral acceleration measurement should be corrected in order to take into account roll angle of the chassis. In an high lateral acceleration condition (e.g. steady state cornering), because of the elastokinematics effect of the suspension, there is vertical loads transfer between left and right wheel axles, the lateral acceleration

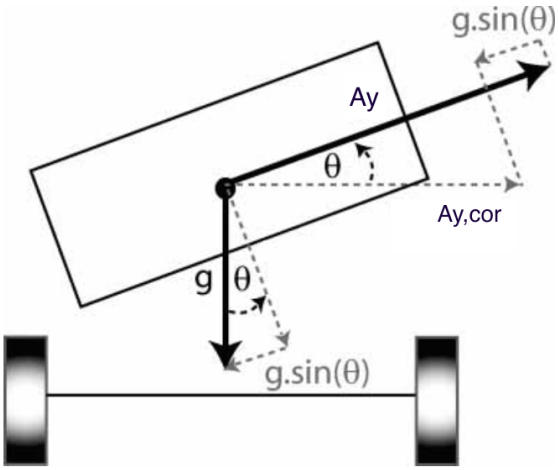

Figure 3.6: Roll angle, lateral acceleration correction

produces an upward angle θ in Figure 3.6, as a consequence that observers produce significant errors.

In the static condition, integrate the roll rate from the measurement has a big drift because the static component noise. So the roll angle can be obtained under the dynamic condition (e.g. sweep input). The lateral acceleration measurement can be corrected according to the vehicle roll angle θ_d. The roll angle θ_d is obtained from the integration of the roll rate $\dot{\theta}_d$ value passing through a high-pass filter, which results in the dynamic roll angle. The ratio between the roll angle θ_d and relative lateral acceleration A_{yd} under dynamic situation is:

$$K = \frac{\theta_d}{A_{yd}} = 8.9 \cdot 10^{-3} \tag{3.12}$$

So the roll angle in steady-state can be obtained as following:

$$\theta_s = K \cdot A_{ys} \tag{3.13}$$

In steady-state cornering, the relation between θ_s and A_{ys} are got in following equation (see Figure 3.6):

$$A_{y,cor} = A_{ys} - g\,sin(\theta_s) = A_{ys} - g\,sin(8.9 \cdot 10^{-3} A_{ys}) \tag{3.14}$$

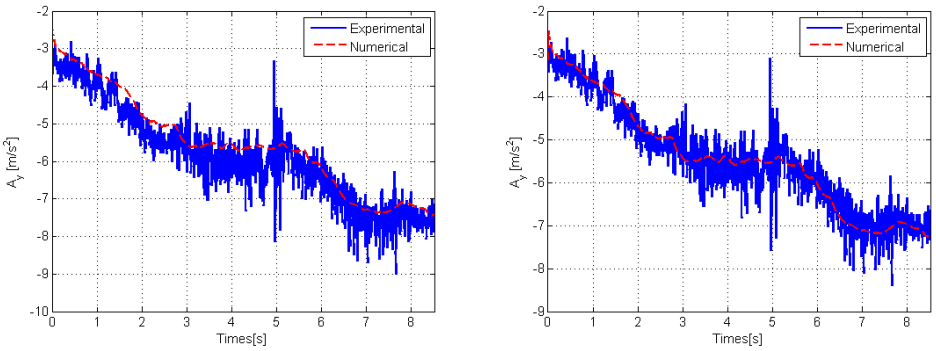

(a) Lateral acceleration before correction (b) Lateral acceleration after correction

Figure 3.7: Lateral acceleration, after the lateral acceleration correction in steady-state input

Figure 3.7 presents lateral acceleration errors after the lateral acceleration correction within a single-track model in a steady-state input. The lateral acceleration errors are significantly reduced. The improvement due to the lateral acceleration correction in relation to the roll variable can clearly be seen for the observer.

Chapter 4

Tyre identification

The chapter proposes an approach to identify the parameters of a tyre model for handling simulation proposes.

The knowledge of tyre parameters is of paramount importance for the correct modelling of vehicle dynamics, in particular for state observer and state estimators.

Tyre parameters can be obtained by different type of tests that can mainly be divided in laboratory tests and outdoor tests. Obviously there are same advantages and disadvantages of both the solutions, the possibility of having a fully instrumented car gives us the possibility of applying the second type of tests.

A single track model vehicle model has applied because it allows plausible description of the lateral dynamics of a vehicle. Also, in order to obtain the wider range of car usage, several tests have been performed both in static and in transient condition as described in the following.

4.1 General approach

The approach for tyre parameters identification is based on the following procedure:

1. Two different type of outdoor tests had been performed
    - Steady state cornering: steering pad constant radius;
    - Sweep sine test at vehicle constant speed.

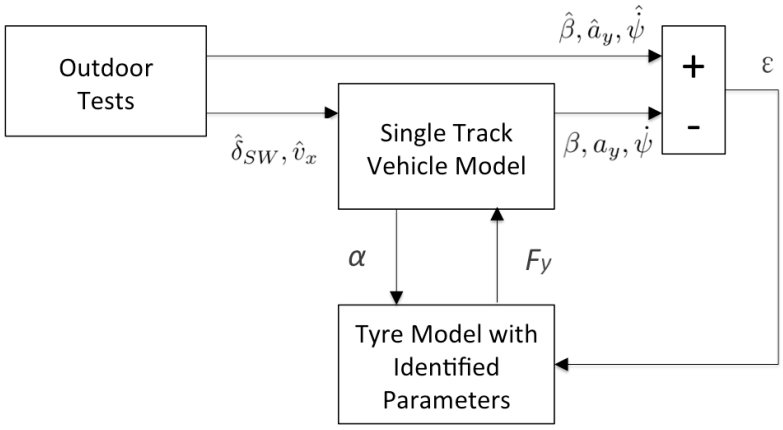

Figure 4.1: Scheme of the procedure used to estimate tyre model parameters

The following measurements of vehicle dynamics are used:

- Vehicle lateral acceleration a_y;
- Vehicle yaw rate $\dot{\psi}$;
- Vehicle longitudinal and lateral velocity v_x and v_y (sideslip angle β);
- Steering-wheel angle δ_{SW};

2. Vehicle simulation is performed using following inputs:
   - Steering-wheel angle δ_{SW};
   - Vehicle longitudinal velocity v_x.
3. Results of simulation in terms of lateral acceleration a_y, yaw rate $\dot{\psi}$ and sideslip angle β are compared with measurements;
4. Tyre parameters are changed in order to reduce the least square error ε between simulation outputs and measurements; the parameters that are thus estimated are:
   - Cornering stiffness $K_{f/r}$;
   - Relaxation length σ.

To better understand the procedures, it has been schematised in Figure 4.1.

4.2 Outdoor tests

To obtain tyre model parameters, this test procedure has to be considered: to get a good approximation, steady-state and transient behaviour can be recognised in different manoeuvres to obtain the lateral condition, so as to judge the steering properties under normal conditions and the stability of the car for high lateral accelerations, the following tests are performed:

- Steering pad constant radius manoeuvre for steady-state behaviour;
- Steer sweep at constant vehicle speed for transient behaviour.

According to the two manoeuvres performed, tyre model, as is explained in the following, is adapted to the manoeuvre itself in order to reduce the number of variables free to change in the minimisation process. This leads to better results and less computation time.

4.2.1 Steering pad constant radius

The steering pad constant radius is performed according to ISO 4138 with the limitation, due to the test facilities, of a maximum radius is about 14 metres. The car is driven with low longitudinal acceleration in order to guarantee quasi-static condition, i.e. longitudinal acceleration increases less than 1 $(m/s^2)/s$. To the end, the max lateral acceleration is measured.

4.2.2 Steer sweep

The car reaches a constant speed of 50 km/h in sweep with cruise control activated, then suddenly rotates the steering wheel to the desired angle, sweeps the steering wheel sharply to the other side under the same angle, follows this routine with several times. In this process, sweep in a small lateral acceleration to make sure the transient condition fulfilled.

4.3 Vehicle model

A single-track vehicle model Figure 4.2 considers the vehicle chassis as a rigid beam with three degrees of freedom in the plane; each axle collects the contact

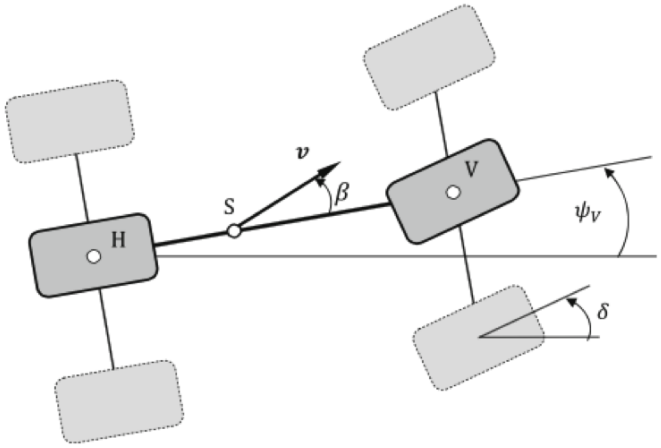

Figure 4.2: Single-track vehicle model

properties of the respective pair of tyres and can present a relative rotation (steer angle) with respect to the vehicle chassis.

The equation of motion of the vehicle are

$$\begin{cases} ma_y = F_{y,f}\cos\delta + F_{y,r} \\ J\ddot{\psi} = F_{y,f}\,a\cos\delta + F_{y,r}\,b \end{cases} \tag{4.1}$$

where m is the vehicle overall mass, J is the yaw moment of inertia, δ is the steer angle of the front axle, a and b are the distances of the c.o.g. from the front and rear axle respectively. Lateral forces of axles depends on many parameters, as described in the following; slip angles of the axles (α_f and α_r) are calculated by following equations:

$$\alpha_f = \arctan\left(\frac{-(v_y + a\dot{\psi})\cos\delta + v_x\sin\delta}{(v_y + a\dot{\psi})\sin\delta + v_x\cos\delta}\right) \tag{4.2}$$

$$\alpha_r = \arctan\left(\frac{-v_y + a\dot{\psi}}{v_x}\right) \tag{4.3}$$

4.4 Tyre model

The tyre model here adopted relies on Pacejka MF-Tyre with five parameters. The Magic Formula tyre model has been developed to achieve an accurate description of steady state tyre behaviour.

The lateral force of tyre $\bar{F}_y$ in steady state condition is obtained by the following equation

$$\bar{F}_y = D \sin\{C \arctan[B\alpha - E(B\alpha - \arctan(B\alpha))]\} \tag{4.4}$$

where α is the slip angle of the considered axle and B, C, D and E are tyre parameters related to $F_y(\alpha)$ vs α curve:

- D represents the maximum value reached by F_y vs α characteristic;
- C is a shape factor;
- BCD represents the slope of the curve at the origin and it's named cornering stiffness;
- B is named stiffness factor;
- E is another shape factor that influences the curvature near the maximum and fixes the position of the maximum itself along the alpha axes.

When forced with a sudden step slip-angle input, the tyre doesn't react immediately with the value of lateral force F_y corresponding to that value of slip angle on the steady-state characteristic, but reaches it with a certain time-lag. In order to take into account the tyre dynamics, a first order time lag model is considered, thus the lateral tyre force F_y is obtained integrating the following differential equation

$$\frac{\sigma}{v_x}\dot{F}_y + F_y = \bar{F}_y \tag{4.5}$$

where σ is the relaxation length of the tyre (which has to be estimated by here described procedure), v_x is the longitudinal speed of the vehicle, and $\bar{F}_y$ is the force calculated with MF, which is the steady-state value of F_y.

4.5 Minimisation procedure

In order to estimate tyre parameter several simulations are performed in a minimisation process driven by `fmincon` function of `Matlab`. The function calls the `Simulink` model of the vehicle and tyres changing tyre parameters in order to minimise the objective function described in the following. The input to vehicle model

Table 4.1: Tyre parameters values and boundaries within the minimisation process

B_f	C_f	D_f	E_f	σ_f	B_r	C_r	D_r	E_r	σ_r
$[2-200]$	1.3	$0.9F_{z,f}$	-0.9	-	$[2-200]$	1.3	$F_{z,r}$	-0.9	-

Table 4.2: Tyre parameters values and boundaries within the minimisation process

B_f	C_f	D_f	E_f	σ_f	B_r	C_r	D_r	E_r	σ_r
$[2-200]$	1.3	$0.9F_{z,f}$	-0.9	[0.3-1.5]	[2-200]	1.3	$F_{z,r}$	-0.9	[0.3-1.5]

are measured steering-wheel angle δ_{SW}, longitudinal vehicle speed v_x. The output of the simulation are lateral acceleration a_y, yaw rate $\dot{\psi}$ and sideslip angle β thus the minimisation is performed in order to obtain the minimum value of the following objective function

$$f(x) = \frac{A_{y\,m} - A_{y\,s}}{max(\| A_{y\,m} \|)} + \frac{\dot{\psi}_m - \dot{\psi}_s}{max(\| \dot{\psi}_m \|)} + \frac{\beta_m - \beta_s}{max(\| \beta_m \|)} \tag{4.6}$$

where $\bullet_m$ stands for measured quantities while $\bullet_s$ stands for simulated quantities.

Tyre parameter C, D and E, of both the axles, are fixed. In steering pad manoeuvre, also σ is fixed while B is free to vary within defined boundaries. This choice is made in order to simplify the minimisation procedure also because there is non influence of σ in tyre behaviour in steady-state cornering conditions. Thus with steady-state cornering the B parameter, i.e. cornering stiffness is obtained. In sweep test instead also relaxation length σ is left free to vary within defined boundaries. The values chosen for fixed parameters and for boundaries are reported in Table 4.1 and Table 4.2 with resptect to front and rear axles.

4.6 Minimisation Results

Among the two kind of experimental tests, steering pad and sweep, the tyre parameters can be found by minimisation method, they are stiffness factor B in the steady-state manoeuvre, stiffness factor B and relaxation length σ in the sweep manoeuvre. After that, the cornering stiffness K is obtained equal to BCD.

In this part, the simulation results are presented on two ways: figures of nu-

merical simulations and experimental measurements, and tables of normalised errors.

In the steering pad test, the vehicle performed a circular trajectory, the one input data steering wheel angle δ are slowly increasing from 150 deg to 168 deg, because the under-steer condition, and the longitudinal velocity v_x is increasing with small longitudinal acceleration.

In the sweep test, the vehicle is running on the straight road, with the sweep input, which the steering wheel input is at the range of 0-60 deg, and always at a constant velocity of 50 km/h.

4.6.1 Steering pad

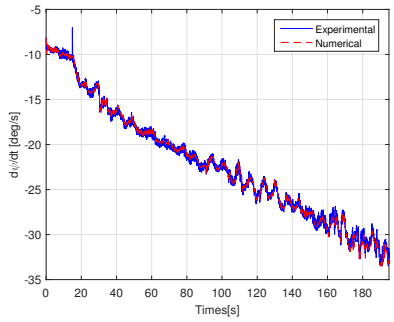

(a) Yaw rate in comparison

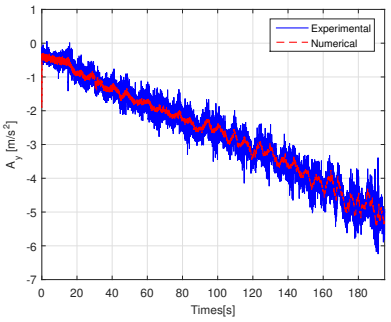

(b) Lateral acceleration in comparison

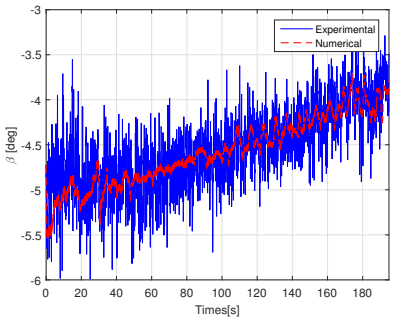

(c) Sideslip angle in comparison

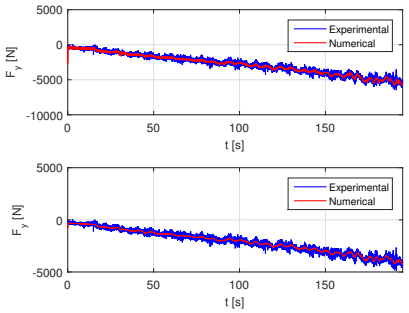

(d) Lateral force of each axle in comparison

Figure 4.3: Steering pad in comparison with experimental measurement

Figure 4.3 shows the steering pad result, the simulation results are relatively satisfactory. The yaw rate $\dot{\psi}$ in Figure 4.3a, lateral acceleration a_y in Figure 4.3b

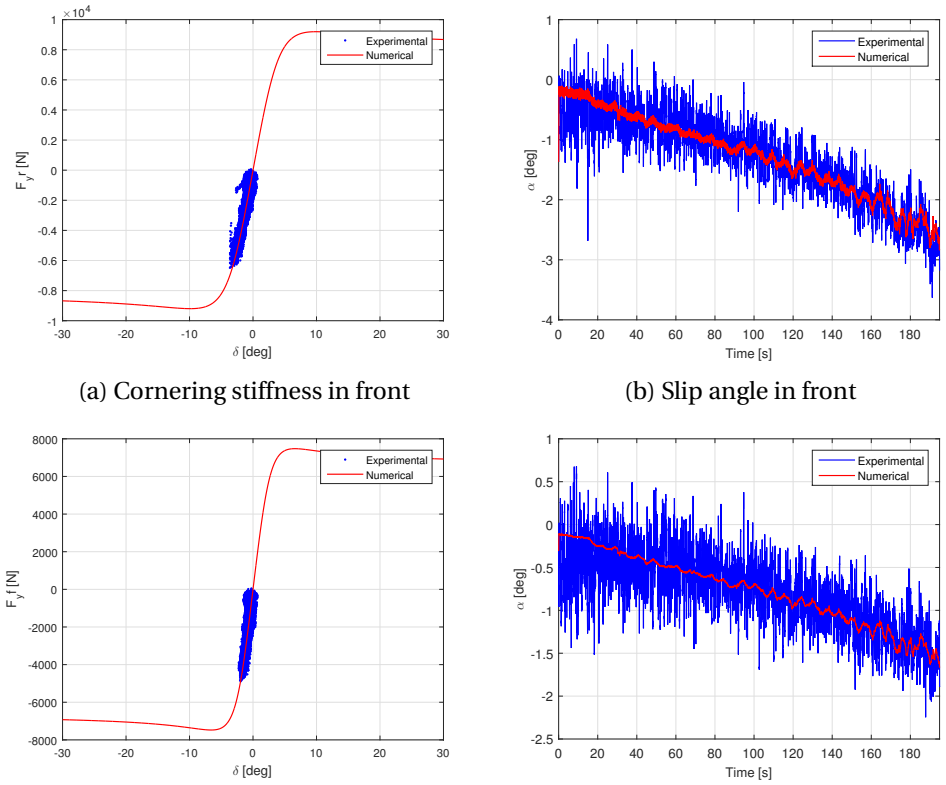

(a) Cornering stiffness in front

(b) Slip angle in front

(c) Cornering stiffness in rear

(d) Slip angle in rear

Figure 4.4: Steering pad cornering stiffness and slip angle in minimum least-square result of both front and rear wheel

and sideslip angle β in Figure 4.3c, who decide the minimisation process, differences between the experimental results and the numerical results are quite small. In figure 4.3d, shows the lateral force of each axle comparison both in front and rear axles, the error is 2.38 % and 1.87 % in Table 4.3.

In Figure 4.4, the converged cornering stiffness K has implemented to give several vehicle state results with comparison. Cornering stiffness of front wheel is shown in Figure 4.4a, the numerical curve passed trough the experimental zone in the middle. Slip angle in front reached the maximum 3.8 deg, but also shows a well matched result in Figure 4.4b. Figure 4.4c and Figure 4.4d are got in the rear wheel, the experimental and numerical data are quite matched, but the cornering stiffness is bigger, and also the slip angle is less than the front wheel. The cornering stiffness results are recorded in Table 4.4.

Table 4.3: Steering pad test, maximum absolute values and normalised mean errors (experiments)

Steering pad	Max(‖‖)	Error(%)
$\dot{\psi}$	34 deg/s	2.34
a_y	5.94 m/s^2	3.12
β	3.85 °	3.20
F_f	5083 N	2.38
F_r	4342 N	1.87
α_f	2.32 °	3.95
α_r	0.77 °	2.29

Table 4.4: Cornering stiffness in Steering pad

Wheel	$K(BCD)$
Front wheel	11.75
Rear wheel	21.56

4.6.2 Sweep sine test

In the sweep test, the relaxation length is also in consideration. In the Figure 4.5, the simulation produces satisfactory results, yaw rate $\dot{\psi}$ in Figure 4.5a, lateral acceleration a_y in Figure 4.5b and sideslip angle β in Figure 4.5c, which are close to measurements. Figure 4.5d gives a quite matched result in lateral force of front and rear axle, but there is still a little delay of the numerical data because the inertial moment of the vehicle can not be perfectly measured by limitation facilities, about 0.1 s delay.

In Figure 4.6, the relative cornering stiffness K has implemented into the calculation. Although the lateral acceleration is less than the one in steering pad, the slip angle of the front and the rear wheel are also well matched (normalised mean errors are around 3 % in Table 4.5). The cornering stiffness and relaxation length value in sweep are in the Table 4.6.

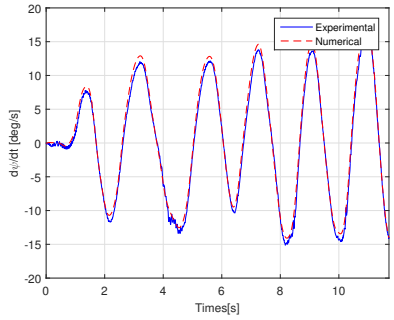

(a) Yaw rate in comparison

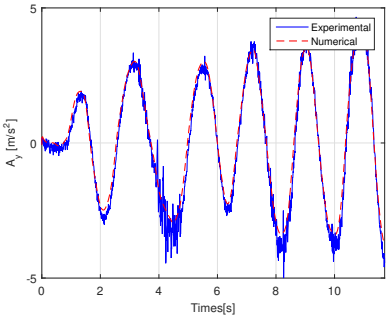

(b) Lateral acceleration in comparison

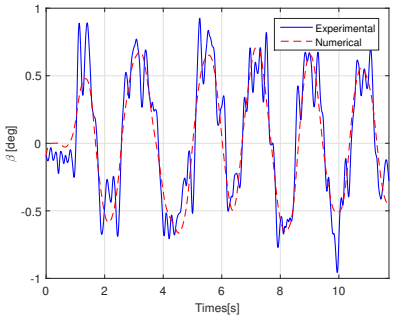

(c) Sideslip angle in comparison

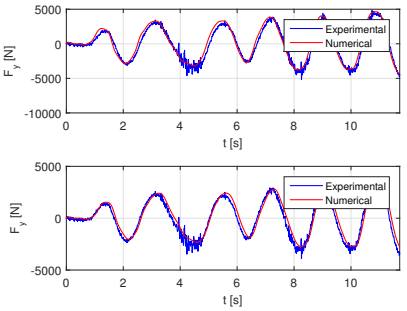

(d) Lateral force of each axle in comparison

Figure 4.5: Sweep in comparison with experimental measurement

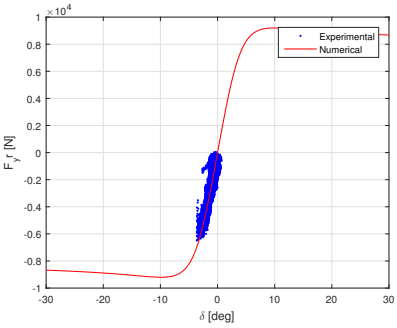

(a) Cornering stiffness in front

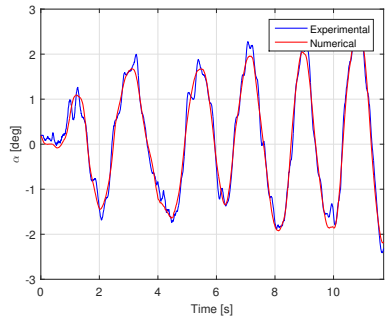

(b) Slip angle in front

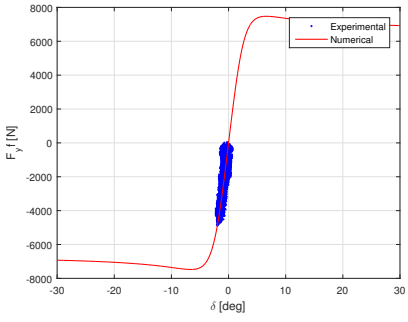

(c) Cornering stiffness in rear

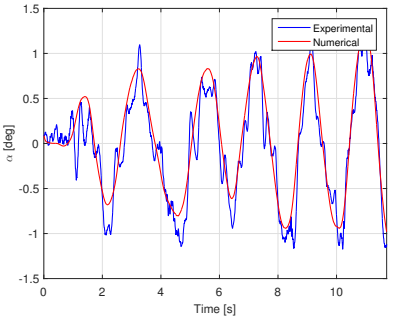

(d) Slip angle in rear

Figure 4.6: Sweep cornering stiffness and slip angle in minimum least-square result of both front and rear wheel

Table 4.5: Sweep test, maximum absolute values and normalised mean errors (experiments)

Steering pad	Max(‖‖)	Error(%)
$\dot{\psi}$	15.21 deg/s	4.30
a_y	3.95 m/s^2	2.65
β	0.76 °	6.32
F_f	3576 N	4.56
F_r	2360 N	3.65
α_f	2.07 °	3.64
α_r	0.97 °	4.57

Table 4.6: Cornering stiffness and relaxation length in sweep

Wheel	$K(BCD)$	Relaxation length
Front wheel	12.32	0.56 m
Rear wheel	22.53	0.67 m

From the two manoeuvres, we can conclude that the mean cornering stiffness is K_f= 11.98, K_r=22.04. The front relaxation length σ_f is 0.56m, the rear one is σ_r is 0.67m.

Chapter 5

Sideslip angle estimation

As is well known, the direct measurement of vehicle sideslip angle requires a complex experimental set-up (an optical device might be used), which does not appear to be suitable for implementation on ordinary passenger cars. But sideslip angle can provide important information for stability control systems. Thus, this quantity has to be estimated.

The Extended Kalman Filter has appied to estimate the sidelipe angle starting of the measurements got from on-vehicle laboratory Data Acquisition system. The Extended Kalman Filter can be regarded as a noise filter and state observer, so the unknown parameter like sideslip angle can be estimated by this algorithm.

5.1 Extended Kalman Filter

The model is based on a non linear single-track vehicle model whose equations of model are:

$$mA_y = F_{wf}cos\delta + F_{wr} \tag{5.1}$$

$$J_z\ddot{\psi} = aF_{wf}\delta - bF_{wr} \tag{5.2}$$

If use the state vector and input vector as following:

$$\underline{x} = \begin{Bmatrix} \beta \\ \dot{\psi} \end{Bmatrix} \quad \underline{u} = \begin{Bmatrix} \delta \\ V \end{Bmatrix} \tag{5.3}$$

The state-space equations of motion of single-track vehicle model becomes

$$\begin{cases} \underline{\dot{x}}(t) = \begin{Bmatrix} \dot{\beta} \\ \ddot{\psi} \end{Bmatrix} = \begin{Bmatrix} -\frac{a_x \beta}{V} - \dot{\psi} + \frac{F_{yf} \cdot cos\delta + F_{yr}}{mV} \\ \frac{aF_{yf} \cdot cos\delta - bF_{yr}}{J_z} \end{Bmatrix} = f(\underline{x}(t), \underline{u}(t)) + w(t) \\ \underline{y}(t) = \begin{Bmatrix} a_y \\ \dot{\psi} \\ \frac{F_{yf}}{F_{zf}} \\ \frac{F_{yr}}{F_{zr}} \end{Bmatrix} = \begin{Bmatrix} \frac{F_{yf}+F_{yr}}{m} \\ \dot{\psi} \\ \frac{F_{yf}}{F_{zf}} \\ \frac{F_{yr}}{F_{zr}} \end{Bmatrix} = h(\underline{x}(t), \underline{u}(t)) + v(t) \end{cases} \tag{5.4}$$

$\underline{y}(t)$ is the measurement vector containing the vehicle lateral acceleration a_y and yaw rate $\dot{\psi}$, and the stochastic terms $\omega(t)$ and $v(t)$ have been added to account for process noise and measurement noise. They are modelled as zero-mean independent white noise processes with known intensity.

Define the augmented state vector of the EKF as:

$$\underline{x}_a = \begin{Bmatrix} \underline{x} \\ \mu \end{Bmatrix} \tag{5.5}$$

μ is the unknown parameter and assumed that the variation of unknown μ can be modeled as white noise

$$\dot{\mu} = w_\mu \tag{5.6}$$

Then, the augmented state-space equation can be rewritten as:

$$\begin{cases} \underline{\dot{x}}_a(t) = \begin{bmatrix} f(\underline{x}(t), \underline{u}(t), \mu(t)) \\ 0 \end{bmatrix} + \begin{bmatrix} w(t) \\ w_\mu \end{bmatrix} \\ \underline{y}(t) = h(\underline{x}(t), \underline{u}(t), \mu(t)) + v(t) \end{cases} \tag{5.7}$$

The EKF in Figure 5.1 is a recursive algorithm that provides a minimum mean-square error estimate $\underline{\hat{x}}_a(t)$ of the state vector $\underline{x}(t)$ and the parameters μ by minimizing the error of error measurement vector. In this application, the EKF equa-

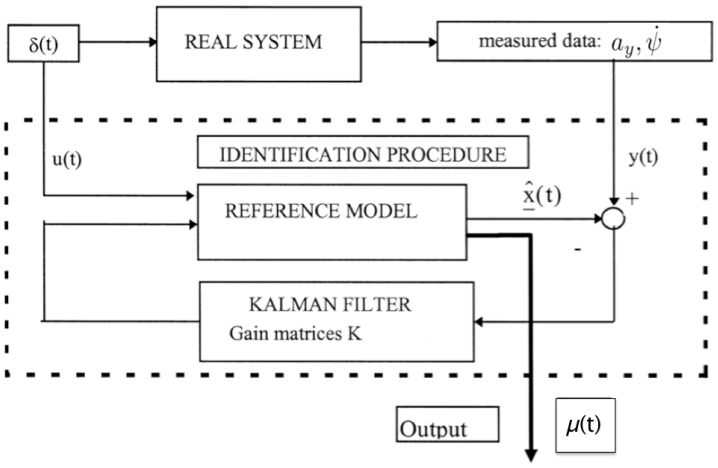

Figure 5.1: EKF

tions become:

$$\begin{cases} \dot{\hat{x}}_a(t) = f(\hat{x}(t), u(t), \hat{\mu}(t)) + \boldsymbol{K}(y(t) - \hat{y}(t)) \\ \hat{y}(t) = h(\hat{x}(t), u(t)) \end{cases} \tag{5.8}$$

where $\boldsymbol{K}$ is the gain matrices. It depends on the solution of a suitable differential matrix Riccati equation, whose coefficients are computed by linearizing Equation around the actual estimated value $\hat{x}(t)$.

In Continuous-time extended Kalman filter, Kalman Gain K and the predicted covariance P are:

$$K = PC^{\mathrm{T}}R^{-1} \tag{5.9}$$

$$\dot{P} = AP - PCR^{\mathrm{T}}CP + Q + PA^{\mathrm{T}} \tag{5.10}$$

where Q is the matrix of the noise variance on the state and R is the matrix of variance of the measurement noise.

The matrices A, B, C and D are obtained by linearising the system with respect

to each state variables.

$$A = \begin{bmatrix} \frac{\partial f_1}{\partial \beta} & \frac{\partial f_1}{\partial \dot{\psi}} & \frac{\partial f_1}{\partial \mu} \\ \frac{\partial f_2}{\partial \beta} & \frac{\partial f_2}{\partial \dot{\psi}} & \frac{\partial f_2}{\partial \mu} \\ 0 & 0 & 0 \end{bmatrix} \quad B = \begin{bmatrix} \frac{\partial f_1}{\partial \delta} & \frac{\partial f_1}{\partial V} \\ \frac{\partial f_2}{\partial \delta} & \frac{\partial f_2}{\partial V} \end{bmatrix} \quad C = \begin{bmatrix} \frac{\partial h_1}{\partial \beta} & \frac{\partial h_1}{\partial \dot{\psi}} & \frac{\partial h_1}{\partial \mu} \\ \frac{\partial h_2}{\partial \beta} & \frac{\partial h_2}{\partial \dot{\psi}} & \frac{\partial h_2}{\partial \mu} \\ \frac{\partial h_3}{\partial \beta} & \frac{\partial h_3}{\partial \dot{\psi}} & \frac{\partial h_3}{\partial \mu} \\ \frac{\partial h_4}{\partial \beta} & \frac{\partial h_4}{\partial \dot{\psi}} & \frac{\partial h_4}{\partial \mu} \end{bmatrix} \quad D = \begin{bmatrix} \frac{\partial h_1}{\partial \delta} & \frac{\partial h_1}{\partial V} \\ \frac{\partial h_2}{\partial \delta} & \frac{\partial h_2}{\partial V} \\ \frac{\partial h_3}{\partial \delta} & \frac{\partial h_3}{\partial V} \\ \frac{\partial h_4}{\partial \delta} & \frac{\partial h_4}{\partial V} \end{bmatrix} \tag{5.11}$$

The only non-linearity is given by the relationship between the contact forces and state variables. Assuming that extended forces are functions only depend on slip angle of each axle (α_f and α_r) and the friction coefficient μ, we have:

$$\begin{aligned} \frac{\partial F_{yf}}{\partial \beta} &= \frac{\partial F_{yf}}{\partial \alpha_f}\frac{\partial \alpha_f}{\partial \beta} & \frac{\partial F_{yf}}{\partial \dot{\psi}} &= \frac{\partial F_{yf}}{\partial \alpha_f}\frac{\partial \alpha_f}{\partial \dot{\psi}} \\ \frac{\partial F_{yr}}{\partial \beta} &= \frac{\partial F_{yr}}{\partial \alpha_r}\frac{\partial \alpha_r}{\partial \beta} & \frac{\partial F_{yr}}{\partial \dot{\psi}} &= \frac{\partial F_{yr}}{\partial \alpha_f}\frac{\partial \alpha_r}{\partial \dot{\psi}} \end{aligned} \tag{5.12}$$

The wheel slip angles have relations below:

$$\alpha_f = \delta - \beta - \frac{\dot{\psi}\cdot a}{V} \qquad \alpha_r = \beta - \frac{\dot{\psi}\cdot b}{V} \tag{5.13}$$

So, defined the result of lateral forces you can write matrices A and C:

$$A = \begin{bmatrix} -\frac{1}{mV}\left(\frac{\partial F_{yf}}{\partial \alpha_f} + \frac{\partial F_{yr}}{\partial \alpha_r}\right) - \frac{A_x}{V} & -\frac{1}{mV^2}\left(a\frac{\partial F_{yf}}{\partial \alpha_f} - b\frac{\partial F_{yr}}{\partial \alpha_r}\right) - 1 & \frac{1}{mV}\left(\frac{\partial F_{yf}}{\partial \mu} + \frac{\partial F_{yr}}{\partial \mu}\right) \\ -\frac{1}{J_z}\left(a\frac{\partial F_{yf}}{\partial \alpha_f} - b\frac{\partial F_{yr}}{\partial \alpha_r}\right) & -\frac{1}{J_z V}\left(a^2\frac{\partial F_{yf}}{\partial \alpha_f} + b^2\frac{\partial F_{yr}}{\partial \alpha_r}\right) & \frac{1}{J_z}\left(a\frac{\partial F_{yf}}{\partial \mu} - b\frac{\partial F_{yr}}{\partial \mu}\right) \\ 0 & 0 & 0 \end{bmatrix} \tag{5.14}$$

$$C = \begin{bmatrix} -\frac{1}{m}\left(\frac{\partial F_{yf}}{\partial \alpha_f} + \frac{\partial F_{yr}}{\partial \alpha_r}\right) & -\frac{1}{mV}\left(a\frac{\partial F_{yf}}{\partial \alpha_f} - b\frac{\partial F_{yr}}{\partial \alpha_r}\right) & \frac{1}{m}\left(\frac{\partial F_{yf}}{\partial \mu} + \frac{\partial F_{yr}}{\partial \mu}\right) \\ 0 & 1 & 0 \\ -\frac{L}{mgb}\frac{\partial F_{yf}}{\partial \alpha_f} & -\frac{aL}{mgbV}\frac{\partial F_{yf}}{\partial \alpha_f} & \frac{L}{mgb}\frac{\partial F_{yf}}{\partial \mu} \\ -\frac{L}{mga}\frac{\partial F_{yr}}{\partial \alpha_r} & \frac{bL}{mgaV}\frac{\partial F_{yr}}{\partial \alpha_r} & \frac{L}{mga}\frac{\partial F_{yr}}{\partial \mu} \end{bmatrix} \tag{5.15}$$

Since the identification is off-line the entyre set of data $\underline{x}_a(t)$ can be processed repeatedly in order to discount the effect of an arbitrary initialization, until convergence is eventually reached.

5.2 Compare with experimental result

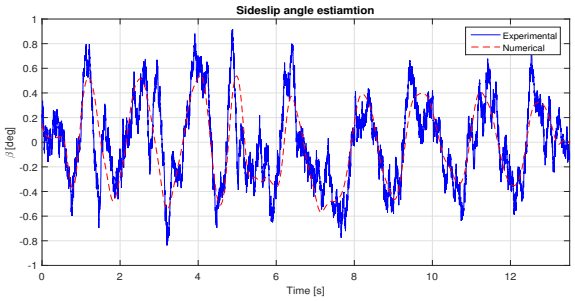

Figure 5.2: Side slip estimation in sweep

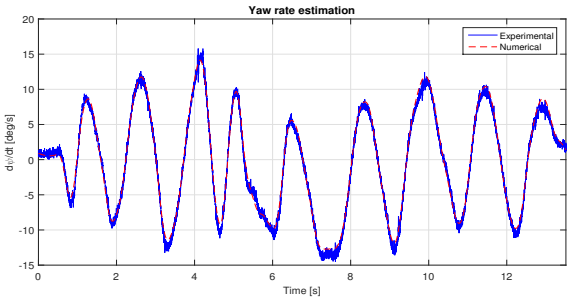

Figure 5.3: Yaw rate estimation in sweep

The estimation process is applied and compared with real experimental data that is obtained from the logged real-time data. The cornering stiffness is defined in the previous chapter about tyre parameters identification, which comprises a fixed linear force model, as a fixed value, K_f is defined as 11.98, whereas K_r is 22.04.

Figure 5.2 shows sideslip angle estimation results for the sweep test. It shows that estimator gives good results with error about 4.73 % when cornering stiffness is approximately known. In real case, if cornering stiffness is reduced, it overestimates rear sideslip angle, whereas if cornering stiffness is increased, the rear sideslip angle is overestimated. Figure 5.3 shows the yaw rate estimation, it can conclude the observer can chase a good result of the experimental data (normalised error is 2.45%). Table 5.1 shows the errors between the simulation and experimental data.

Table 5.1: Sweep tests, maximum absolute values and normalised mean errors (experiments)

Estimation	Max of measurement ($\|\|$)	Mean error(%)
Sideslip(β)	0.78 °	4.73
Yaw rate($\dot{\psi}$)	15.13 °/s	2.45

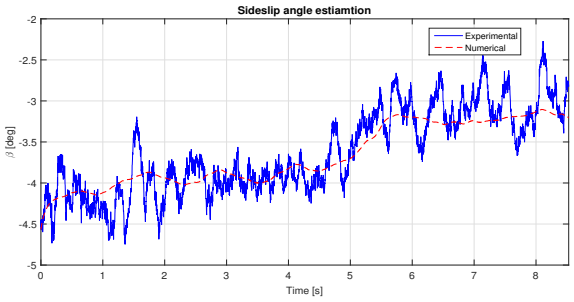

Figure 5.4: Side slip estimation in steering pad

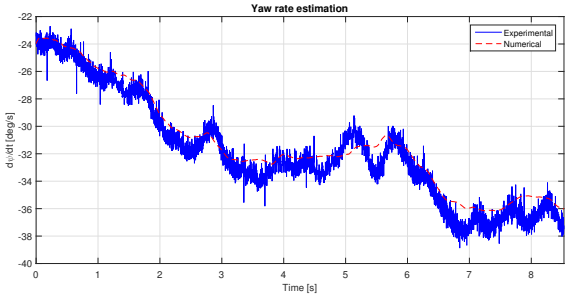

Figure 5.5: Yaw rate estimation in steering pad

Table 5.2: Steering pad tests, maximum absolute values and normalised mean errors (experiments)

Estimaion	Max of measurement ($\|\|$)	Mean error(%)
Sideslip(β)	4.50 °	3.21
Yaw rate($\dot{\psi}$)	37.41 °/s	1.52

Figures 5.4, Figure 5.5 and Table 5.2 present estimation results for steering pad test. Sideslip angle is very large (round about 4.5°), however it is well estimated by the observer when the cornering stiffness is known. Moreover, in the steering pad test steering angle and vertical loads transfer are high, this induce large elastokinematics effects, correction of the lateral acceleration has applied into the observer to decrease the error.

Chapter 6

Conclusion

An Data Acquisition system is introduced for drivers and engineers to take measurements, analyse data, and display the results. In the thesis, a CAN BUS communication system has been developed, which can also store data transmitted from the vehicle on-board computer, allowing time-synchronized storage of vehicle computer data with the measured from Data Acquisition system.

Then the article shows the potential of the two estimation processes. The first presents the estimation of parameters in Magic Formula tyre-force model, whereas the second supplies sideslip angle estimation.

The used non linear least square optimization method is suitable for the determination of the Magic Formula parameters. The thesis presents results obtained from two driving tests (steering pad and sweep). Based on the single-track model. Cornering stiffness estimation is satisfactory in the major part of tests, notably in the sweep tests. However, in the steering pad tests (in the case of high steering angle and high load transfer), the roll angle correction is necessary to take in consideration in order to decrease the estimation errors.

In the estimation of the sideslip process, the Extended Kalman Filter is successfully estimated the sideslip angle and yaw rate, both with the small normalised mean errors.

Of course certain improvements are desirable. During the tests have been performed, the manoeuvres can not achieve the maximum of the tire map because of the limitation of the test facilities, also the vehicle itself can not give a better performance. When the model can reach the peak force value of the tyre, the simulation

can be more accurate. Then will be the investigate the expansion of the vehicle model to include lateral load transfer effect, to separate the axle lateral force more accurately between the two tyres.

In EKF part, the results are well matched under the fixed cornering stiffness, however this assumption also needs to be confirmed with more experimental tests in various road surfaces. Future, improve the model with an adaptive tire-force model should be taken into consideration, which is robust when cornering stiffness parameters change and can give sideslip angle estimations more close to measurements.

Appendix A

Nomenclature

Symbol	Description
g	Gravitational constant (m/s^2)
J_z	Yaw moment of inertia (Kg/m^2)
a	Centre of gravity to front axle distance (m)
b	Centre of gravity to rear axle distance (m)
m	Vehicle mass (Kg)
L	vehicle wheelbase (m)
v	Centre of gravity vehicle speed (m/s)
a_x, a_y	longitudinal, lateral acceleration (m/s^2)
x, u, y	State, input, measurement, vectors
x_a, y_a	Extended state, measurement, vectors
μ	Road friction coefficient
β	Centre of gravity sideslip angle (rad)
α_f	Front sideslip angle (rad)
α_r	Rear sideslip angle (rad)
δ	Steering angle (rad)
$\dot{\psi}$	Yaw rate (rad/s)
θ	Roll angle (rad)
L_f, L_r	Front, rear wheel relaxation length (m)
BCD	Cornering stiffness (N/rad)
F_{yf}, F_{yr}	Lateral front, rear tire forces

Bibliography

[1] Anton T Van Zanten. Evolution of electronic control systems for improving the vehicle dynamic behavior. In *Proceedings of the 6th International Symposium on Advanced Vehicle Control*, pages 1–9, 2002.

[2] Charles M Farmer, Adrian K Lund, Rebecca E Trempel, and Elisa R Braver. Fatal crashes of passenger vehicles before and after adding antilock braking systems. *Accident Analysis & Prevention*, 29(6):745–757, 1997.

[3] Hans Pacejka. *Tire and vehicle dynamics*. Elsevier, 2005.

[4] F Braghin, F Cheli, and E Sabbioni. Environmental effects on pacejka's scaling factors. *Vehicle System Dynamics*, 44(7):547–568, 2006.

[5] P Bolzern, F Cheli, G Falciola, and F Resta. Identification from rapid vehicle manoeuvres of the equivalent suspension-tire cornering forces. In *CESA'96 IMACS Multiconference: computational engineering in systems applications*, pages 903–908, 1996.

[6] Anton T Van Zanten, Rainer Erhardt, Georg Pfaff, Friedrich Kost, Uwe Hartmann, and Thomas Ehret. Control aspects of the bosch-vdc. In *AVEC*, volume 96, pages 573–608, 1996.

[7] Aleksander Hac and Melinda D Simpson. Estimation of vehicle side slip angle and yaw rate. Technical report, SAE Technical Paper, 2000.

[8] Paul J TH Venhovens and Karl Naab. Vehicle dynamics estimation using kalman filters. *Vehicle System Dynamics*, 32(2-3):171–184, 1999.

[9] MA Wilkin, WJ Manning, DA Crolla, and MC Levesley. Use of an extended kalman filter as a robust tyre force estimator. *Vehicle System Dynamics*, 44(sup1):50–59, 2006.

[10] Matt C Best, TJ Gordon, and PJ Dixon. An extended adaptive kalman filter for real-time state estimation of vehicle handling dynamics. *Vehicle System Dynamics*, 34(1):57–75, 2000.